Modulated Structure of $TaSi_{0.414}Te_2$: Sandwich Stacking in the MA_xTe_2 (M = Nb, Ta; A = Si, Ge; $^1/_3 \leq x \leq {}^1/_2$) Series

M. Evain,* A. van der Lee, and L. Monconduit

IMN, Laboratoire de Chimie des Solides, UMR CNRS No. 110, Université de Nantes, 2, rue de la Houssinière, 44072 Nantes Cédex 03, France

V. Petříček

Institute of Physics, Academy of Sciences of the Czech Republic, Na Slovance 2, 180 40 Praha 8, Czech Republic

Received March 31, 1994. Revised Manuscript Received June 6, 1994®

The complete structure of the incommensurate compound $TaSi_{0.414}Te_2$ has been determined by single-crystal X-ray diffraction. The (3 + 1)D superspace group is $Pnma(00\gamma)s00$, $\gamma = 0.414(1)$, basic unit-cell dimensions $a = 6.318(1)$, $b = 14.031(2)$, $c = 3.8552(7)$ Å, $V = 341.8(1)$ Å^3, and $Z = 4$. Refinement on 2989 reflections with $I \geq 2.5\sigma(I)$ converged to $R = 0.111$, $R = 0.054$ for 1100 main reflections and $R = 0.113$, 0.164, 0.325, and 0.527 for 1270 first-order, 311 second-order, 179 third-order, and 129 fourth- and sixth-order satellites, respectively. The structure can be considered as a succession of commensurate domains of the $TaSi_{3/7}Te_2$ and $TaSi_{2/5}Te_2$ structures. Although demonstrated as being incommensurate, the structure is compared to the closest, simple hypothetical commensurate structure, $TaSi_{5/12}Te_2$. A detailed analysis of the sandwich stacking in the MA_xTe_2 series, $^1/_3 \leq x \leq {}^1/_2$, is performed. Stacking rules are established and a symmetry versus stacking relationship is discussed.

Introduction

Within the frame of a systematic study of the charge transfer processes in the MA_xTe_2 family of compounds (M = Nb, Ta; A = Si, Ge; $^1/_3 \leq x \leq {}^1/_2$), several noteworthy features have already been found.[1-11] MA_xTe_2 compounds have sandwich-like structures with the same intrasandwich basic unit cell, containing four face-sharing trigonal prisms of Te, a statistically occupied A-site in the center of the rectangular face common to two trigonal prisms, and two independent M sites in the centers of two trigonal prisms, whose occupancies sum up to exactly 1 (Figure 1).

The difference between the compounds stems from the setting-up of different x-dependent superstructures and from different sandwich stacking arrangements. For certain values of x the difference between a long-period superstructure and a true incommensurate phase cannot any longer be made. One of those phases, $TaSi_{0.414}Te_2$, is the subject of this paper.

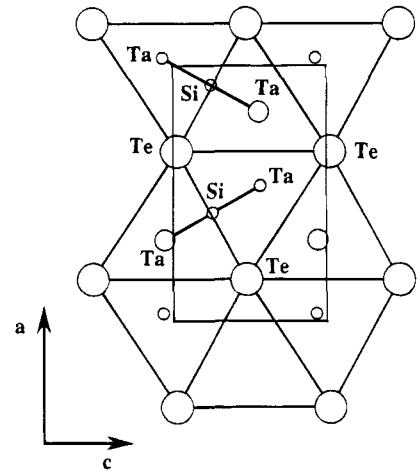

Figure 1. Projection of one sandwich of the basic unit cell of the $TaSi_{0.414}Te_2$ modulated structure. Te atoms form a hexagonal network; Ta atoms pairs and Si atoms are lone. The radius of the circles representing the atoms is proportional to their occupation probability.

The modulation primarily develops from a cationic ordering over the available sites within the sandwiches. Associated with the occupational modulation of M and A is a displacive modulation of all atoms.[5] Most M atoms are bonded together to form M-M pairs. The remaining nonbonded M atoms form zigzag strips that demarcate the regions where M–M bonding takes place. Short Te–Te contacts (~3.3 Å, substantially shorter than the sum of the van der Waals radii 4.1 Å) are found for all x, within and parallel to the sandwiches just above and below the M–M bonds. These slightly

* To whom correspondence should be addressed.

® Abstract published in *Advance ACS Abstracts,* July 15, 1994.

(1) Monconduit, L.; Evain, M.; Boucher, F.; Brec, R.; Rouxel, J. *Z. Anorg. Allg. Chem.* **1992**, *616*, 1–6.
(2) Monconduit, L.; Evain, M.; Brec, R.; Rouxel, J.; Canadell, E. *C. R. Acad. Sci. Paris* **1993**, *314*, 25–34.
(3) Li, J.; Caroll, P. J. *Mater. Res. Bull.* **1992**, *27*, 1073–1081.
(4) Li, J.; Badding, M. E.; DiSalvo, F. J. *J. Alloys Comp.* **1992**, *184*, 257–263.
(5) Van der Lee, A.; Evain, M.; Monconduit, L.; Brec, R; Van Smaalen, S. *J. Phys.: Condens. Matter.* **1993**, *6*, 933–944.
(6) Canadell, E.; Monconduit, L.; Evain, M.; Brec, R.; Rouxel, J.; Whangbo, M.-H. *Inorg. Chem.* **1993**, *32*, 10–12.
(7) Van der Lee, A.; Evain, M.; Monconduit, L.; Brec, R.; Rouxel, J.; Petříček, V. *Acta Crystallogr.* **1994**, *B50*, 119–128.
(8) Evain, M.; Monconduit, L.; Van der Lee, A.; Brec, R.; Rouxel, J.; Canadell, E. *New J. Chem.* **1994**, *18*, 215–222.
(9) Van der Lee, A.; Evain, M.; Mansuetto, M.; Monconduit, L.; Brec, R; Rouxel, J. *J. Solid State Chem.*, in press.
(10) Liang, W.; Whangbo, M.-H.; Evain, M.; Monconduit, L.; Brec, R.; Bengel, H.; Cantow, H.-J.; Magonov, S. N. *Chem. Mater.* **1994**, *6*, 678–685.
(11) Rouxel, J; Evain, M. *Eur. J. Solid State Inorg. Chem.*, in press.

0897-4756/94/2806-1776$04.50/0 © 1994 American Chemical Society

bonding contacts imply a charge transfer from the anions to the cations.[6,8] In addition, considerable Te–Te interactions between the [Te/M, A/Te] sandwiches (with distances as short as 3.75 Å) occur in all compounds.[10,11] In addition, there are the curious symmetry changes with x. For $x = 1/3$,[1,3,4,8] $x = 3/7$,[5] $x = 0.3602$,[7] and $x = 0.414$ the complete modulated structure is orthorhombic, whereas for $x = 1/2$[2] and $x = 2/5$[9] a monoclinic symmetry is found. The latter symmetries are not caused by slight distortions of the orthorhombic structure, but correspond to shifts of either the complete sandwich ($x = 1/2$) or the cationic contents of a sandwich over one or more basic unit cells along the c-axis ($x = 2/5$). Since the intrasandwich arrangement is—disregarding the actual length of the modulation wave length—equivalent in all cases ($1/3 \leq x \leq 1/2$), one expects differences in intersandwich bonding to be responsible for the formation of these different three dimensional structures.

To reveal what might cause the symmetry change from monoclinic to orthorhombic by changing the A content by only 4% (i.e., $x = 0.40$ and $x = 0.414$), we undertook the determination of the complete modulated structure of $TaSi_{0.414}Te_2$. The refinement procedure employs the principles of the superspace group formalism.[12] In addition a new technique for the modelling of displacive modulation functions is introduced and applied.[13] The discussion will focus on the sandwich stacking of all known compounds of the MA_xTe_2 series in relation to their symmetry and the Te–Te short contact pattern.

Experimental Section

The compound $TaSi_{0.414}Te_2$ was prepared from a mixture of the elemental powders (Ta, Fluka 99.7%; Si, Aldrich 99%; Te, Fluka 99.7%) in the ratio Ta:Si:Te = 7:3:14. The mixture was ground and loaded into a quartz tube. The tube was evacuated to 10^{-2} Torr, sealed, and placed in a programmable furnace. The temperature of the furnace was raised from room temperature to 1250 K at 100 K/h, kept fixed for 10 days, and then cooled to ambient temperature at 100 K/h.

Small, very thin platelets with a metallic luster were found in the batch. A semiquantitative SEM analysis yielded a composition $Ta_{0.83}Si_{0.63}Te_2$. It should be noted that the proportions of Ta and Si are difficult to extract from the spectrum, because of the overlap of the Ta K-emission peak and the Si L-emission peak. The title composition $TaSi_{0.414}Te_2$ is therefore based on the refinement results and structural arguments.

Weissenberg films showed a primitive orthorhombic lattice of main reflections with $a \approx 6.3$, $b \approx 14.0$, and $c \approx 3.9$ Å, thus similar to that found in the other MA_xTe_2 compounds. In addition to the main spots, a sublattice of weaker spots could be identified corresponding to a 5-fold superstructure along the c axis ($\mathbf{q} = 2/5\mathbf{c}^*$). The crystal was then mounted on an Enraf-Nonius CAD-4F diffractometer. By an accurate centering of some strong first-order satellites, it was detected that the $\mathbf{q}$ vector is actually incommensurate with the underlying main lattice. The final length of the $\mathbf{q}$ vector was least-squares refined with the program U-FIT[14] from the setting angles of 32 first-order satellite reflections: $\mathbf{q} = \gamma\mathbf{c}^* = 0.4144(10)\mathbf{c}^*$. It is noted that γ is equal to the rational value $\gamma' = 5/12$ within 3 standard deviations.

Data collection of main reflections was subsequently performed, followed by that of satellite reflections up to the sixth order. Table 1 compiles the recording conditions; Table 2 contains some reflection statistics. The measured intensities were corrected for a small drift variation monitored by three reference reflections (<1%), for Lorentz and polarization effects, and for absorption using some programs of the XTAL system.[15] The absorption correction is very sensitive to an accurate determination of the thickness of the platelet. It was optimized by repeating the final refinements with data sets obtained with slightly different thicknesses until a minimal R value was reached.

Symmetry-related reflections were averaged according to Laue symmetry *mmm*, because the superspace

Table 1. Crystal Data of $TaSi_{0.414}Te_2$ and Measurement Conditions

formula	$TaSi_{0.414}Te_2$
formula weight (amu)	447.79
density (calc)	8.761
$F(000)$	731
linear absorption coefficient	511.0 cm^{-1}
crystal size	$<0.09 \times 0.004 \times 0.09$ cm^3
maximum correction	12.9
minimum correction	1.5
superspace group	$Pnma(00\gamma)s00$
basic unit cell	$a = 6.318(1)$ Å
	$b = 14.031(2)$ Å
	$c = 3.8552(7)$ Å
	vol = 341.8(1) $Å^3$
modulation vector	$\mathbf{q} = 0.4144(10)\mathbf{c}^*$
diffractometer	CAD-4F
temperature	295 K
radiation	Mo K–$L_{2,3}$
scan mode	$\omega/(2\theta)$

		h_{min}	h_{max}	k_{min}	k_{max}	l_{min}	l_{max}
hklmn range	main	0	10	−24	24	0	6
	1st order	0	8	−19	19	0	5
	2nd order	0	8	0	19	0	6
	3th order	0	8	0	19	0	6
	4th order	0	8	0	19	0	7
	6th order	0	6	0	13	0	6
standard reflections		(2300), (2$\bar{3}$00), (3010) every hour					

Table 2. Reflection Statistics[a]

	N_1	N_2	$\langle I \rangle$	$\langle I/\sigma(I) \rangle$
main	1782	1100	100.0	14.7
1st order	1886	1270	41.4	13.9
2nd order	927	311	9.8	6.8
3th order	823	179	5.3	4.7
4th order	739	103	11.1	7.1
6th order	199	26	6.4	5.3
all	6356	2989	56.1	12.6

[a] N_1 is the total number of data collected, N_2 is the number of data with $I \geq 2.5\sigma(I)$. $\langle I \rangle$ and $\langle I/\sigma(I) \rangle$ are calculated for the N_2 data. The values in the column for $\langle I \rangle$ are normalized to 100.0 for the strongest reflection class. The internal R factor for averaging in Laue class *mmm* is 0.039: 1859 unique reflections are left for refinement.

(12) See for a technical treatment of superspace group theory, e.g., §9.8 in *International Tables for Crystallography* Vol. C; Wilson, A. J. C., Ed.; Kluwer Academic Publishers: Dordrecht, **1992**. A more descriptive treatment is given by, e.g.: Janssen, T.; Janner, A. *Adv. Phys.* **1987**, *36*, 519–624.

(13) Petříček, V.; Van der Lee, A. *Acta Crystallogr.*, submitted.

(14) Evain, M. U-FIT: A cell parameter refinement program, 1992, Institut des Matériaux de Nantes, Nantes, France.

(15) Hall, S. R., Flack, H. D., Stewart, J. M., Eds. Xtal3.2 Reference Manual, 1992, Universities of Western Australia, Geneva, and Maryland.

group describing the modulated structure was assumed to be similar to that of $TaSi_{0.360}Te_2$.[7] The systematic absent reflections found in the diffraction pattern were in accordance with this assumption. The nonlinear least-squares refinements (described in the next paragraph) were performed with the JANA93 computing system.[16] The scattering factors for neutral atoms and the anomalous dispersion correction were taken from the International Tables for X-ray Crystallography.[17] All refinements were based on $|F_{obs}|$ and performed in a full-matrix mode, using unit weights for all reflections.

Structure Refinement. The symmetry of incommensurately and long-period modulated structures is usually described by $(3 + n)$D superspace groups[12] where n $(1 \leq n \leq 3)$ gives the number of modulation wave vectors necessary to obtain an integer indexing of the diffraction pattern. In the present case $n = 1$; the satellite reflections along $\mathbf{c}^*$ are indexed by an integer m in addition to the normal set of Miller indices (hkl) according to

$$\mathbf{H} = h\mathbf{a}^* + k\mathbf{b}^* + l\mathbf{c}^* + m\mathbf{q}$$

with $\mathbf{H}$ the diffraction vector; $\mathbf{a}^*$, $\mathbf{b}^*$, and $\mathbf{c}^*$ the reciprocal axes, and $\mathbf{q}$ the modulation wave vector. The symmetry of the modulated structure of $TaSi_{0.414}Te_2$ is, like that of $TaSi_{0.360}Te_2$, described by the $(3 + 1)$D superspace group $Pnma(00\gamma)s00$ with $\gamma = 0.414$. This can be deduced from the observed systematic extinctions for the reflections $(hklm)$.[12]

The determination and refinement of an incommensurately modulated structure is usually a two-step procedure. First, the "average" structure is refined using the main reflections $(hkl0)$ only, and second, the modulation is determined using the main reflections and the satellite reflections. The modulations of the atomic coordinates and/or the site occupancy probability are mostly described by Fourier series:

$$\mathbf{r}^{\nu}(\bar{x}_4) = \mathbf{r}_0{}^{\nu} + \sum_{n=1}^{n_{max}} (\mathbf{u}^{\nu}_{s,n} \sin(2\pi n\bar{x}_4) + \mathbf{u}^{\nu}_{c,n} \cos(2\pi n\bar{x}_4))$$

$$\mathbf{P}^{\nu}(\bar{x}_4) = \mathbf{P}_0{}^{\nu} + \sum_{n=1}^{n_{max}} (\mathbf{P}^{\nu}_{s,n} \sin(2\pi n\bar{x}_4) + \mathbf{P}^{\nu}_{c,n} \cos(2\pi n\bar{x}_4))$$

where $\mathbf{r}_0{}^{\nu}$ and $P_0{}^{\nu}$ are the basic structure coordinate and the site occupancy probability, respectively, for atom ν. The number of harmonics in the refinement, n_{max}, is usually equal to the highest order of the observed satellite reflections. The argument of the modulation function, $\bar{x}_4$, is defined as follows: $\bar{x}_4 = t + \mathbf{q}\cdot\mathbf{r}^{\nu}_{0,\mathbf{L}} = t + \mathbf{q}\cdot(\mathbf{r}_0{}^{\nu} + \mathbf{L})$, with t the global phase of the modulation wave ($t = 0$ is used for the refinements in the present work), and $\mathbf{L}$ a basic structure lattice translation. The goal of a modulated structure determination is to find the Fourier amplitudes $\mathbf{u}^{\nu}_{s,n} = (A^{\nu}_{x,s,n}, A^{\nu}_{y,s,n}, A^{\nu}_{z,s,n})$, $\mathbf{u}^{\nu}_{c,n} = (A^{\nu}_{x,c,n}, A^{\nu}_{y,c,n}, A^{\nu}_{z,c,n})$, and $P^{\nu}_{x,n}$ and $P^{\nu}_{c,n}$. We have shown before that the occupancy modulations is quite often better modeled by a crenel function than by a Fourier series.[7] This function is defined by

$$\mathbf{P}^{\nu}(\bar{x}_4) = H(\bar{x}_4 - \bar{x}^{\nu}_{4,l}) - H(\bar{x}_4 - \bar{x}^{\nu}_{4,r})$$

where $H(x) = 0$ if $x < 0$, and $H(x) = 1$ if $x > 0$; $\bar{x}^{\nu}_{4,l} = \bar{x}^{\nu}_{4,0} - \Delta^{\nu}/2$ and $\bar{x}^{\nu}_{4,r} = \bar{x}^{\nu}_{4,0} + \Delta^{\nu}/2$; Δ^{ν}, the width of the step, is just equal to the average occupation probability $P_0{}^{\nu}$, and $\bar{x}^{\nu}_{4,0}$ represents the center of the step.

It is obvious that interatomic distances modulate as well and that there is, because of the incommensurability, an infinite number of such distances for each pair of atoms of the average structure. Therefore, the information concerning interatomic distances in a modulated structure is best presented by a plot of distance versus t in the interval [0;1]; in this way all distances present in the modulated structure are given at the same time (see Figures 3 and 4).

The refinements proceeded along the same lines as that for $TaSi_{0.360}Te_2$ with one major modification. Here we give only a brief summary and a short description of the modification; for details we refer to the paper on $TaSi_{0.360}Te_2$.[7]

The parameters of the average structure, keeping the Debye–Waller parameters isotropic, refined to a final R factor of 0.18 ($wR = 0.18$). The refinement of the modulated structure was initiated with low-order Fourier components for the modeling of the displacive modulation waves of all atoms and with step functions for the occupational modulation waves of the cations. Only one step function parameter was refined; the centers $\bar{x}^{\nu}_{4,0}$ of Ta(2) and Si were constrained to that of Ta(1) in such a way that the occupancy of the cationic sites of the basic unit cell would never lead to unrealistic short distances. The equation to fulfill this requirement is

$$\bar{x}^{\nu}_{4,0} = \bar{x}^{Ta(1)}_{4,0} + \gamma(z^{\nu} - z^{Ta(1)}) - 0.5 \qquad \nu = Ta(2), Si(1)$$

Refinements performed in this way suffered from heavy correlations between Fourier amplitudes of different order. Moreover, the refinement of the displacive parameters of Si was very unstable, causing shifts to unreasonable values without any physical meaning.

This problem finds its origin in the occupational nature of the modulation. The displacive modulation functions are not properly defined for those intervals of the phase of the modulation where the occupational modulation functions are exactly zero. In other words, the distinct harmonics of the displacive modulation functions are no longer orthogonal but become linearly dependent. The obvious remedy for this problem is a reorthogonalization of the displacive modulation functions over the interval where the occupational modulation functions take the value one. The Fourier amplitudes $\mathbf{u}^{\nu,ort}_{s,n}$ and $\mathbf{u}^{\nu,ort}_{c,n}$ of the orthogonalized functions can be subsequently used in the least-squares matrix. The details of the implementation of this orthogonalization procedure will be described in a forthcoming paper.[13]

Using the new Fourier amplitudes, the majority of the heavy correlations vanished, and the Si position remained reasonably stable. The refinement results are compiled in Table 3. Table 3 also contains the Fourier amplitudes of the original functions corresponding to the new ones obtained from the refinement. The former are easier to manipulate than the latter, for instance

(16) Petříček, V. JANA93: programs for modulated and composite crystals, 1993, Institute of Physics, Praha, Czech Republic.

(17) Cromer, D. T.; Waber, J. T. In *International Tables for X-ray Crystallography*; Ibers, J. A., Hamilton; W. C., Eds.; Kynoch Press: Birmingham, England, 1974; Vol. IV, pp 72–98. Cromer, D. T. *Ibid.* pp 149–150.

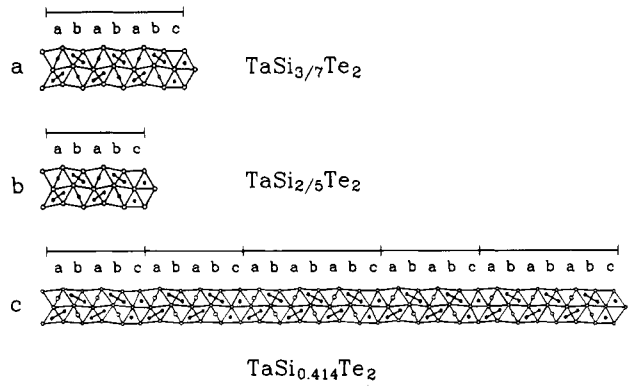

Figure 2. Ordering pattern of $[TaSi_{3/7}Te_2]$ (a) and $[TaSi_{2/5}Te_2]$ (b) motifs in one $[TaSi_{0.414}Te_2]$ sandwich (c) along the running direction of the modulation wave.

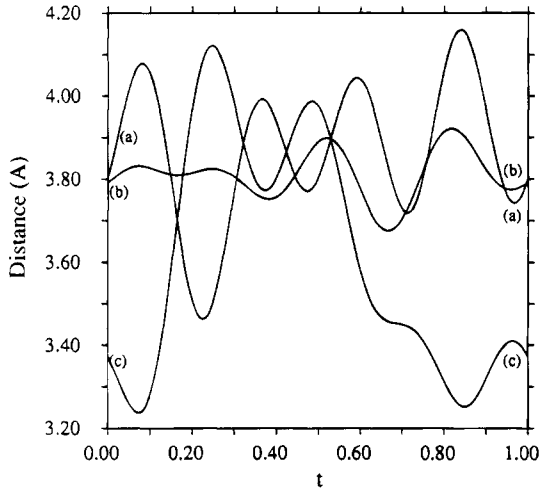

Figure 3. Te–Te distances (Å) parallel to the $[TaSi_{0.414}Te_2]$ sandwich as a function of the phase t of the modulation wave:

	$\langle d \rangle$	d_{min}	d_{max}
(a)	3.868	3.462	4.159
(b)	3.811	3.675	3.922
(c)	3.605	3.237	4.121

for the calculation of atomic positions and bond distances. Note that the Fourier amplitudes of the nonorthogonalized functions sometimes take very large values, and that the "mean", i.e. $\mathbf{u}^{\nu}_{c,0}$, does not correspond to the average coordinates. They are just the zeroth-order term in the Fourier expansion.

In the Experimental Section it was already mentioned that the wave vector is, within 3 standard deviations, commensurate with the underlying basic lattice. To test the possible commensurability, we have performed refinements using the commensurate wave vector. Indeed, using the refinement results of Table 3 one finds a quasi-12-fold periodicity along the c-axis (*vide infra*). The 3D symmetry of this twelve-fold superstructure is $P2_1/m$. This is in perfect agreement with predictions in a previous paper[5] that the n-glide plane that is present in *Pmma* cannot be retained in an even-fold superstructure. The three possible symmetries for an n-fold (n even) superstructure of the parent superspace group $Pnma(00\gamma)s00$ are $P2_1/m$ for global phases $t_0 = 0$ (mod 1/2n), $P2_1ma$ for $t_0 = 1/4n$ (mod 1/2n), and Pm otherwise. To perform the refinement of this monoclinic superstructure the superspace group $P2_1/m(00\gamma)$ was chosen. For the commensurate case the same problems related to the orthogonalization of the displacive modulation functions as for the incommensurate case occur, but now for discrete functions instead of continuous ones. A discrete version of the orthogonalization procedure was developed and applied in the least-squares refinement. Note that the number of atoms, and accordingly the number of parameters, is doubled compared to the incommensurate case. The final R factors for this commensurate model are significantly higher than the incommensurate model, especially if the extra number of variables is taken into account (Table 4). However, if the structure is truly incommensurate with γ close the rational value $^5/_{12}$, a significant noncoherent overlap of especially the high-order satellite reflections is expected. This effect is not taken into account in the current approach and probably causes the large partial R factors for the high-order satellites. Thus, with the present crystallographic method it is not easy to decide between commensurateness and incommensurateness. However, complementary studies by means of AFM and STM imaging techniques do suggest an incommensurate modulation rather than a commensurate one.[18] From a crystallographic point of view the two models do not differ much.

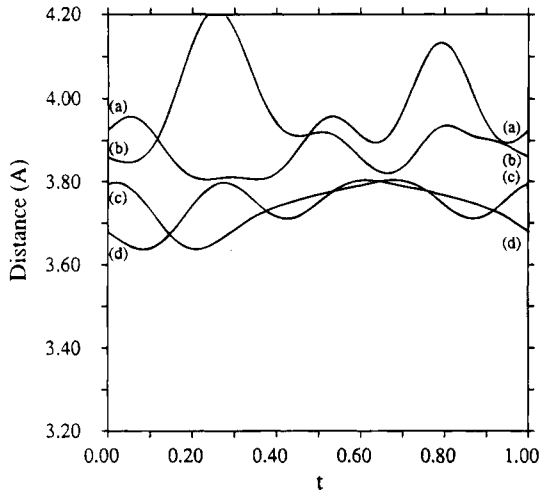

Figure 4. Te–Te distances (Å) perpendicular to the $[TaSi_{0.414}Te_2]$ sandwiches as a function of the phase t of the modulation wave: (a) and (b) interlayer, (c) and (d) intralayer:

	$\langle d \rangle$	d_{min}	d_{max}
(a)	3.919	3.806	4.133
(b)	3.943	3.820	4.210
(c)	3.742	3.638	3.804
(d)	3.742	3.638	3.804

Discussion

Structural Features. The $TaSi_{0.414}Te_2$ structure derives from a hypothetical MoS_2-type $TaTe_2$ structure, as do all MA_xTe_2 structures (M = Nb, Ta; A = Si, Ge; $^1/_3 \leq x \leq {}^1/_2$). The insertion of silicon atoms within the [Te/Ta/Te] sandwich is concomitant with a pairing of some Ta cations, the number of pairs matching the number of silicon atoms introduced according to the formulation $(M_2)_xM_{1-2x}A_xTe_2$ ($^1/_3 \leq x \leq {}^1/_2$).

It has been shown[7] that the wave vector component $\gamma = 0.4144(10)$ is directly related to the A-atom content ($\gamma = x$), and thus the title formula $TaSi_{0.414}Te_2$. As

(18) Bengel, H.-J.; Cantow, H.-J.; Magonov, S. N.; Monconduit, L.; Evain, M.; Liang, W.; Whangbo, M.-H. *Chem. Mater.*, in press.

Table 3. Final Values for the Amplitudes of the Displacive Modulation Functions[a]

	n	$A^{\nu}_{x,s,n}$	$A^{\nu}_{y,s,n}$	$A^{\nu}_{z,s,n}$	$A^{\nu}_{x,c,n}$	$A^{\nu}_{y,c,n}$	$A^{\nu}_{z,c,n}$
Ta(1)	0				0.3163(8)	0.25	−0.047(3)
					0.2862	0.25	0.0391
	1	−0.0075(5)	0.0	−0.0270(8)	0.0004(22)	0.0	−0.0429(3)
		−0.0438	0.0	0.0850	0.0292	0.0	−0.1621
	2	0.006(2)	0.0	−0.010(4)	−0.0004(8)	0.0	0.0034(9)
		0.0291	0.0	−0.0926	−0.0026	0.0	0.0041
	3	−0.002(2)	0.0	0.009(3)	−0.0007(10)	0.0	0.0045(6)
		−0.0057	0.0	0.0249	−0.0042	0.0	0.0277
Ta(2)	0				0.020(2)	0.25	−0.051(5)
					−0.4616	0.25	0.0268
	1	−0.0015(8)	0.0	0.020(3)	−0.017(4)	0.0	0.038(8)
		0.5517	0.0	0.0955	−0.5586	0.0	0.3020
	2	0.016(3)	0.0	−0.025(7)	0.002(1)	0.0	−0.012(1)
		0.3851	0.0	−0.0536	−0.0048	0.0	0.2706
	3	0.006(1)	0.0	−0.007(2)	0.0020(2)	0.0	0.0026(4)
		0.0631	0.0	−0.0886	0.0630	0.0	0.0821
Si	0				0.424(4)	0.25	0.270(7)
					0.4028	0.25	0.2948
	1	−0.005(5)	0.0	0.034(7)	−0.006(6)	0.0	0.010(6)
		−0.0033	0.0	0.0456	−0.0270	0.0	0.0454
Te	0				0.1688(3)	0.1167(1)	0.4739(4)
					0.1670(2)	0.11676(8)	0.4771(3)
	1	0.0249(4)	0.0010(2)	0.0060(7)	0.0224(2)	−0.0014(2)	−0.0113(7)
	2	0.0085(6)	−0.0004(4)	−0.0023(9)	−0.0019(6)	0.0012(3)	0.0190(7)
	3	−0.0099(7)	0.0011(6)	0.0104(9)	0.0050(7)	0.0004(4)	0.0002(10)
	4	0.0048(9)	0.0002(10)	−0.028(1)	0.0088(8)	−0.0003(7)	−0.002(1)

[a] The first line for each order for each atom, except for Te, gives the orthogonalized Fourier amplitudes $\mathbf{u}^{\nu,\mathrm{ort}}_{s,n}$ and $\mathbf{u}^{\nu,\mathrm{ort}}_{c,n}$ that result from the refinement; the second line gives the corresponding nonorthogonalized amplitudes. The latter can be used to calculate atomic coordinates and bond distances according to

$$\mathbf{r}^{\nu}(\bar{x}_4) = \sum_{n=0}^{n_{\max}} [\mathbf{u}^{\nu}_{s,n} \sin(2\pi n\bar{x}_4) + \mathbf{u}^{\nu}_{c,n} \cos(2\pi n\bar{x}_4)]$$

where ν counts the independent atoms in the basic unit cell. The argument of the modulation function has been defined as follows: $\bar{x}_4 = t + \mathbf{q}\cdot\mathbf{r}^{\nu}_{0,\mathrm{L}} = t + \mathbf{q}\cdot(\mathbf{r}_0{}^{\nu} + \mathbf{L})$, with t the global phase of the modulation wave ($t = 0$ is used in the present work), $\mathbf{L}$ a basic structure lattice translation; and $\mathbf{u}^{\nu}_{s,n} = (A^{\nu}_{x,s,n}, A^{\nu}_{y,s,n}, A^{\nu}_{z,s,n})$, $\mathbf{u}^{\nu}_{c,n} = (A^{\nu}_{x,c,n}, A^{\nu}_{y,c,n}, A^{\nu}_{z,c,n})$. The occupational modulation functions are defined as

$$P^{\nu}(\bar{x}_4) = H(\bar{x}_4 - \bar{x}^{\nu}_{4,l}) - H(\bar{x}_4 - \bar{x}^{\nu}_{4,r})$$

where $H(x) = 0$ if $x < 0$ and $H(x) = 1$ if $x > 0$; $\bar{x}^{\nu}_{4,l} = \bar{x}^{\nu}_{4,0} - \Delta^{\nu}/2$ and $\bar{x}^{\nu}_{4,r} = \bar{x}^{\nu}_{4,0} + \Delta^{\nu}/2$; Δ^{ν} the width of the step, is just equal to the average occupation probability and $\bar{x}^{\nu}_{4,0}$ represents the center of the step. As explained in the text, only $\bar{x}^{\mathrm{Ta}(1)}_{4,0}$ was refined: $\bar{x}^{\mathrm{Ta}(1)}_{4,0} = 0.868(8)$.

Table 4. Final Reliability Factors for the Incommensurate and the Commensurate Model[a]

	Pnma(00γ)*s*00 $\gamma = 0.4144$		$P2_1/m$(α0γ) α = 0; $\gamma = {}^5/_{12}$	
	R	wR	R	wR
main	0.054	0.055	0.062	0.062
1st order	0.113	0.149	0.144	0.182
2nd order	0.164	0.189	0.196	0.221
3th order	0.325	0.412	0.318	0.385
4th, 6th order	0.527	0.599	0.401	0.456
overall	0.111	0.126	0.126	0.136

[a] The numbers of unique reflections and independent parameters for the incommensurate model are 1859 and 74, respectively, and for the commensurate model 1989 and 140, respectively.

already stated, γ is close to the rational value $^5/_{12}$ from which one calculates the following formula $(Ta_2)_5Ta_2Si_5Te_{24}$. This last formula can be decomposed as a sum of two simpler terms: $(Ta_2)_3TaSi_3Te_{14}$ ($TaSi_{3/7}Te_2$) and $(Ta_2)_2TaSi_2Te_{10}$ ($TaSi_{2/5}Te_2$) that contain only one lone Ta per formula (i.e., one lone Ta ribbon per sandwich per unit cell). Therefore one expects the sandwich of the $TaSi_{0.414}Te_2$ structure to be, in a first approximation, a succession of $TaSi_{3/7}Te_2$ and $TaSi_{2/5}Te_2$ in-slab basic units. In Figure 2 two such building units (2a and 2b) are presented. In the same figure (2c), a fraction of the unit sequence of the real structure is also shown. One easily notices the regular succession of the two building units, except on the left-hand side of the picture where two $TaSi_{2/5}Te_2$ units are consecutive. This is in agreement with the $TaSi_{0.414}Te_2$ formulation (that is, the wave vector component value $\gamma = 0.414$) that indicates that the structure is very close to that of $TaSi_{5/12}Te_2$ but richer in $TaSi_{2/5}Te_2$ units than in $TaSi_{3/7}Te_2$ structural motifs ($^2/_5 < \gamma < {}^5/_{12} < {}^3/_7$).

In Figures 3 and 4, plots of Te−Te interatomic distances versus the $t = \bar{x}_4 - \vec{\mathbf{q}}\vec{\mathbf{r}}_0{}^{\nu}$ phase of the modulation wave are presented. The main features of such distance variations ($d_{\min}$, $d_{\max}$, and $\langle d\rangle$) are gathered in the figure captions. The most interesting distance is the Te−Te intraslab distance given in Figure 3c. That distance covers three different situations: (i) the Te−Te contacts above the Ta−Ta bonds (that is, the contacts forming an edge of the rectangular faces joining the two trigonal prisms containing the Ta atoms of the Ta−Ta pairs), (ii) the in-plane Te−Te edges on top of the Si atoms (that is, part of the rectangular faces encompassing the Si atoms), and (iii) the Te−Te edges at the limit between two prisms of the [$TaTe_2$] like ribbons (that is, between a prism with a lone Ta and an empty prism). According to the title formula, one expects the various probabilities for the distance to match the three different situations to be 0.414, 0.414, and 0.172, respectively. In the distance plot as a function of t, the probability of finding a distance is directly proportional to the interval on the t axis to which it corresponds. One easily notices the short in-

plane Te–Te contacts ($3.24 < d < 3.45$ Å; $t < 0.12$ and $t > 0.71$) of the first case. The average distance in this range (3.33 Å) is in perfect agreement with the usual distance found in all MA_xTe_2 structures (for instance 3.35 Å in $TaSi_{1/3}Te_2$).[8] That distance, substantially shorter than the sum of the van der Waals radii (4.1 Å) corresponds to bonding contacts.[6,8] These are referenced as type I short contacts hereafter. On the same curve (c of Figure 3), the lengthening of the Te–Te contact ($3.70 < d < 4.12$ Å; $0.16 < t < 0.57$) coincides with the second situation, i.e., the surrounding of the Si atoms. Here again, the average distance, 3.92 Å, is very similar to what is found in $TaSi_{1/3}Te_2$ (3.96 Å). The remaining intervals, $0.12 < t < 0.16$ and $0.57 < t < 0.71$, give the distance range $3.45 < d < 3.70$ Å ($d_{avg} = 3.51$ Å) for the last Te–Te contact type, within the $[TaTe_2]$ like ribbons. Again, it is in perfect agreement with the equivalent distance in $TaSi_{1/3}Te_2$ (3.54 Å). The other distance fluctuations presented in Figures 3 and 4 are not easily interpretable. Let us just mention the shortest interlayer Te–Te contacts of 3.8 Å (Figure 4a). Those contacts through the van der Waals gap (referenced as type II short contacts) are a constant of the MA_xTe_2 structures (3.84 Å in $TaSi_{1/3}Te_2$) although their character gradually shift from antibonding when $x = 1/2$ to bonding when $x = 1/3$.[11] They are the signature of the sandwich–sandwich interaction and could be the clue to the understanding of the stacking rules in the MA_xTe_2 series, which we will now consider.

Stacking Rules in the MA_xTe_2 Series. To understand the stacking of the $[MA_xTe_2]$ layers, let us first analyze the cases of the end members of the series: $MA_{1/3}Te_2$ and $MA_{1/2}Te_2$. In Figure 5 (a and b) is presented in a schematic way the projection of one layer and of two layers, respectively, of such compounds. To untangle the projection view of the layer stacking, the Te atoms involved in type I or type II short contacts (vide supra) are separated out in Figure 5c. Type I contacts always occur in pairs, in an "eclipsed", parallel arrangement (the Te(I–II–I) units) or an "alternate", parallel way (the Te(I–I) units). A type II short contact always links the two pairs of a Te(I–II–I) unit (thus the Te(I–II–I) label). An alternative picture is that presented in Figure 5d where the metal atoms have been isolated. To the Te(I–II–I) and the Te(I–I) units correspond easily identifiable M_2 pair motifs labeled M(I–II–I) and M(I–I), respectively. Notice that, since the type II Te–Te short contacts are always linked with the Te(I–II–I) units in a one to one correspondence, they are associated to the M(I–II–I) motifs as well. Finally, in Figure 5e both the Te atoms, the M atoms, and the links already included in Figure 5c,d are drawn. It is worth noticing that each Te atom of a Te(I–II–I) unit is just on top of an M atom (paired or unpaired) of the neighboring sandwich but that each Te atom of the Te(I–I) group faces an empty prism of the adjacent sandwich. The type II Te–Te short contacts accross the van der Waals gap always occur when there is a perfect matching between the type I Te–Te short contacts and the metals of the adjacent sandwich. This seems to be the requisite feature for a proper anchorage of one sandwich to another.

The various stacking features observed for the end members of the MA_xTe_2 series, that is, $MA_{1/3}Te_2$ and $MA_{1/2}Te_2$, apply to all members known so far, i.e., for

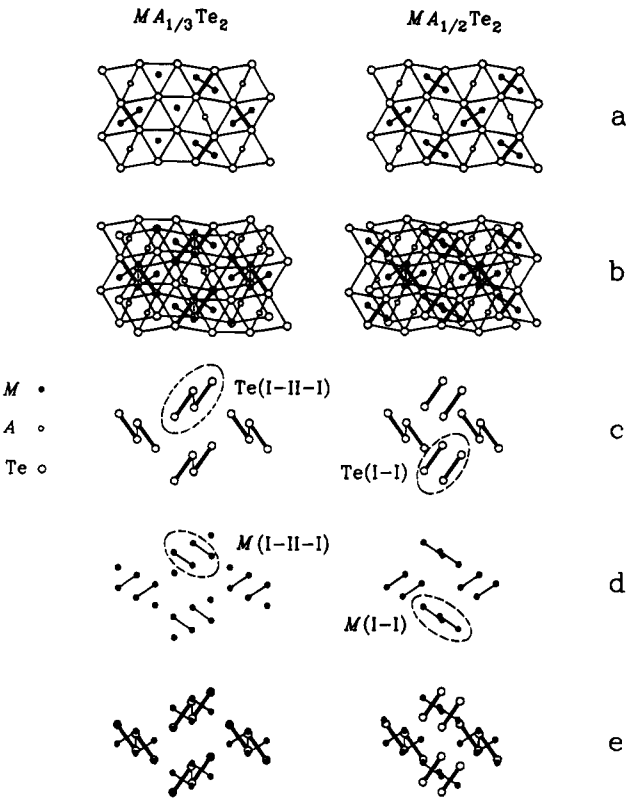

Figure 5. Stacking principles in the MA_xTe_2 series exemplified by the two end members of the family: $MA_{1/3}Te_2$ and $MA_{1/2}Te_2$. (a and b) projections of one and two MA_xTe_2 sandwiches, respectively; (c) type I (within the sandwiches, thick line) and type II (in between the sandwiches, thin line) short Te–Te contacts, isolated from (b), that occur in two different motifs: Te(I–II–I) and Te(I–I); (d) M atoms, isolated from (b), with M_2 pairs and lone M atoms. A one to one correspondence is made between the M_2 pairs pattern and the Te–Te short contacts in (c), thus the labelling of the M_2 pairs motifs: M(I–II–I) and M(I–I); (e) superposition of the (c) and (d) sandwich projection fragments showing the perfect matching between the Te atoms of the Te(I–II–I) motifs and the M atoms of the neighbor sandwich and the absence of M atoms on top, or below, the Te atoms of the Te(I–I) motifs.

MA_xTe_2 $x = 1/2$, $3/7$, 0.414, $2/5$, 0.360, and $1/3$ (the $4/11$ case is not taken into account since it differs in building units and slab pattern[19]). The fact that all type I Te–Te short contacts couple, in projection, in only two ways, either Te(I–II–I) or Te(I–I), was checked for each structure, irrespective of the value of γ of each phase (see Figure 6 for a schematic view of the alternate projection with the M(I–II–I) and M(I–I) motifs). From that analysis, a formula giving the number of Te(I–II–I) and Te(I–I) groups per MA_xTe_2 formula as a function of x is established:

$$n_{Te(I-II-I)} = (1 - x)/2 \qquad n_{Te(I-I)} = (3x - 1)/2$$

An extended formulation can then be proposed for the MA_xTe_2 compounds: $(M_2)_xA_x[Te_2]_{(1-x)}[Te_2]_{(3x-1)}M_{1-2x}Te_{2(1-2x)}$ ($1/3 \le x \le 1/2$) where the different Te atoms refer to Te in the Te(I–II–I) groups, Te in the Te(I–I) motifs, and other Te not involved in the type I short contacts, respectively (the brackets denote type I short Te–Te contacts). This formula gives a good insight into the building principle of the structure. For instance, for x

(19) Van der Lee, A.; Evain, M.; Monconduit, L.; Brec, R; Petříček, V. *Inorg. Chem.*, in press.

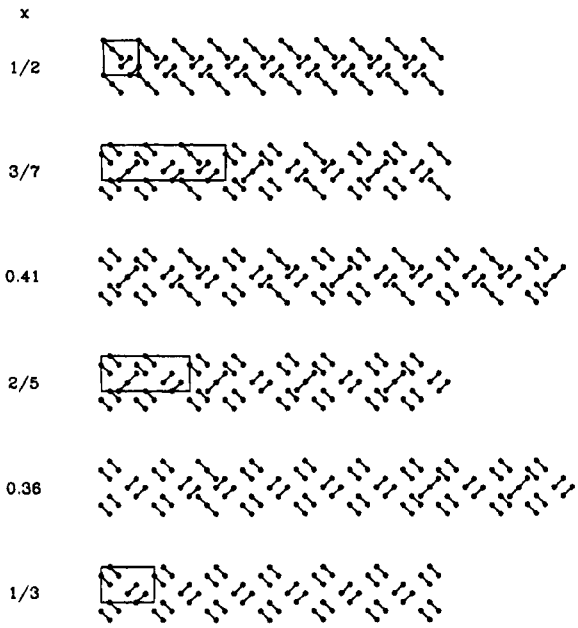

Figure 6. Stacking of two sandwiches as a function of x in the MA_xTe_2 series as a projection of the M_2 pairs. Boxes represent the superstructure unit cells for the commensurate cases. The representation is similar to that given in Figure 5d.

$= 1/2$ it reduces to $(M_2)_{1/2}A_{1/2}[Te_2]_{1/2}[Te_2]_{1/2}M_0Te_0$. This gives useful information: (1) the wave vector component along the running direction is $1/2$, (2) there are no lone M atoms, (3) all Te atoms are engaged in type I short contacts, (4) the Te(I−II−I) and Te(I−I) motifs are in equal proportion, and (5) one quarter of the Te atoms participates in the type II intersandwich short contacts. Similarly, for $x = 2/5$, one obtains $(M_2)_{2/5}A_{2/5}[Te_2]_{3/5}[Te_2]_{1/5}M_{1/5}Te_{2/5}$. This indicates for instance that 30% of the Te atoms are engaged in the type II short contacts through the van der Waals gap.

Since the Te(I−II−I) and Te(I−I) (or equivalently M(I−II−I) and M(I−I)) patterns are the preferential motifs found in the MA_xTe_2 series, one can easily predict the positioning of one sandwich on top of the adjacent one and, consequently, the symmetry of the modulated structure. For instance, the monoclinic symmetry of $MA_{2/5}Te_2$ can be explained by considering the five possible stackings of two sandwiches in the $MA_{2/5}Te_2$ structure (see Figure 7). It is seen that in the usual *Pnma* stacking (Figure 7a) the M pattern does not match the expected arrangement. By shifting the second slab over either one or four basic units in the c direction (Figure 7b), one obtains the experimental M(I−II−I) and M(I−I) arrangements.[9] Shifting over either two or three basic units (Figure 7c) yields other, nonobserved M(I−II−I) and M(I−I) arrangements. Although the stacking rules give the relative position of two neighboring sandwiches, they cannot predict the final space group symmetries since they cannot differentiate between polytypes as we will now discuss.

Stacking and Symmetry. Let us consider again the $MA_{2/5}Te_2$ stacking example. Starting with one $[MA_{2/5}Te_2]$ layer, one has two possibilities for the positioning of the next sandwich (1 and 4 unit shifts in Figure 7). Since, at this stage, both solution are equivalent, let us choose the one unit shift. For the third sandwich, one has again two possibilities. Now the choice is important since it will lead to two different monoclinic symmetries

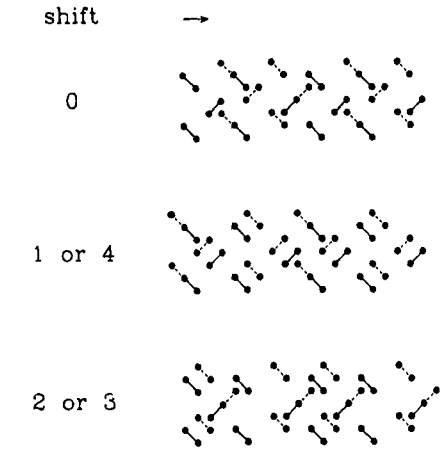

Figure 7. Stacking of two sandwiches in the $MA_{2/5}Te_2$ structure as a function of the basic unit shift of the second slab (arrow). The experimental M(I−II−I) and M(I−I) arrangements are obtained by a shift of either one or four basic units in the c direction, starting from the usual *Pnma* stacking (zero shift).

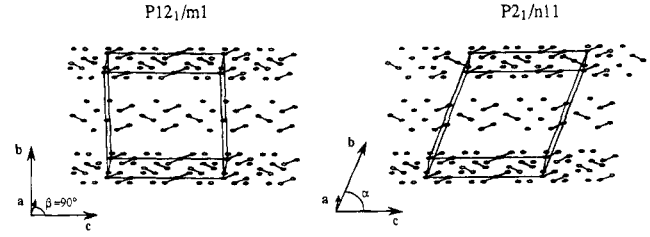

Figure 8. Schematic illustration of the two polytypes possible for the $MA_{2/5}Te_2$ compounds. The filled circles give the actual M atom positions; the open circles correspond to the projection of the middle plane M atoms onto the adjacent planes, perpendicularly to the planes. Such projections show the validity of the stacking rules for both polytypes, that is, the preferential formation of M(I−II−I) and M(I−I) arrangements.

as shown in a schematic way in Figure 8. A four-unit shift can be chosen which gives a monoclinic symmetry (space group $P12_1/m1$, $\alpha = \gamma = 90°$ and $\beta \approx 90°$), but with a pseudoorthorhombic lattice. On the other hand, a one-unit shift leads to a different monoclinic symmetry (space group $P2_1/n11$, $\beta = \gamma = 90°$ and $\alpha \neq 90°$), now with a monoclinic lattice. The latter case corresponds to the obverved one. The structure turns out to be twinned, one domain corresponding to a shift of 1 unit of the second sandwich with respect to the first one, the other domain to a shift of 4 units.[9] In Figure 8, a projection (open circle) of the middle sandwich, perpendicularly to the sandwich plane, onto the upper and lower sandwiches shows that the stacking rules are fulfilled (we only have M(I−II−I) and M(I−I) patterns) for the two polytypes.

Because of the similarity of the basic lattices of all MA_xTe_2 compounds, the only difference being the magnitude of the modulation wave vector, one expects one parent superspace group for all phases. Indeed, $Pnma(00\gamma)s00$ is found for $\gamma = 1/3$, 0.360, $3/7$, and 0.414. The supercell symmetry of the phases $\gamma = 1/3$ and $\gamma = 3/7$ is *Pnma*. The supersymmetry of $MA_{2/5}Te_2$ ($\gamma = 2/5$) would be characterized by $Pnma(00n_1/n_2)s00$ if its supercell symmetry would be $P12_1/m1$.[5] In general, one can show that the supercell symmetry of phases with parent superspace group $Pnma(00n_1/n_2)s00$ is necessarily lower than *Pnma*, if $n_1 + n_2 =$ even, e.g., $P12_1/m1$, but not $P2_1/n11$. Since the latter space group is the

correct space group of the observed $MA_{2/5}Te_2$ phase, its superspace group symmetry cannot be $Pnma(00n_1/n_2)$-$s00$, but instead $P2_1/n(0\beta\gamma)$. Thus, $Pnma(00n_1/n_2)s00$ and $P2_1/n(0\beta\gamma)$ describe the symmetry of two polytypes.

A similar situation is encountered for the $NbSi_{1/2}Te_2$ structure. Indeed, in that structure the stacking rules are fulfilled but the 3D space group ($P112_1/c$, $\gamma \neq 90°$) does not belong to the superspace group $Pnma(00n_1/n_2)$-$s00$.[2,20] Once again, a polytype is obtained, different from that observed for $NbGe_{2/5}Te_2$, that implies a different cation stacking mode, an (AA)(BB)(CC) mode instead of the (AA)(BB) mode which prevails in most MA_xTe_2 phases.

In conclusion, superspace group theory fails to unify the symmetries of all modulated phases of the homologous MA_xTe_2 series to one parent superspace group. The underlying reason is that it cannot take into account a possible polytypism.

Concluding Remarks

The determination of the complete modulated structure of $TaSi_{0.414}Te_2$ confirms the building principles of a sandwich of an incommensurate MA_xTe_2 structure,[7] that is, the quasi periodic succession of two motifs that contitute the repeat unit of the two commensurate structure $MA_{(1+n)/(3+2n)}Te_2$ and $MA_{(1+(1+n))/(3+2(n+1))}Te_2$, $(1 + n)/(3 + 2n) < x < (1 + (1 + n))/(3 + 2(n + 1))$.

(20) Evain, M.; Monconduit, L.; Van der Lee, A., manuscript in preparation.

Previous studies[9,19] on MA_xTe_2 compounds suggested the lone M atom ribbons (MTe_2 blocks or "faults") to play a crucial role in the slab stacking through the establishment of short intersandwich Te−Te contacts. The current, thorough analysis of the stacking rules in the MA_xTe_2 series shows that the anchorage of one sandwich to another might actually be governed by the interaction between the M atoms of one sandwich and the Te atoms of the other sandwich, the faults being not a requisite to such an interaction as exemplified by the $MA_{1/2}Te_2$ structure which presents type II short Te−Te contacts although having no faults.[20]

The question of the true nature of the intrasandwich type I and intersandwich type II Te−Te short contacts remains. Indeed, if their presence is well understood in the $MA_{1/3}Te_2$ phases and interpreted[6,8] as slighly bonding interactions linked to a charge transfer from the cations to the anions according to the $M^{3+}A^{2+}{}_{1/3}Te^{11/6-}{}_2$ oxidation formulation, their role must be clarified in the $MA_{1/2}Te_2$ compounds since those phases are well characterized by the integral oxidation state formulation $M^{3+}A^{2+}{}_{1/2}Te^{2-}{}_2$. A new electronic structure study is under way.

Acknowledgment. The research of AvdL has been made possible by a grant from the C.N.R.S (Sciences Chimiques) and that of VP by the Grant 202/93/1154 from the Grant Agency of the Czech Republic.

Supplementary Material Available: Listing of thermal parameters (1 page); *hklm* observed and calculated structure factors (11 pages). Ordering information is given on any current masthead page.